Antiferromagnetic Spin-Correlations in the Zn-Mg-Ho Icosahedral Quasicrystal

Taku J Sato, Hiroyuki Takakura and An Pang Tsai
*National Research Institute for Metals, Tsukuba 305-0047, Japan,**
and CREST, Japan Science and Technology Corporation, Saitama 332-0012, Japan

Kaoru Shibata and Kenji Ohoyama
Institute for Materials Research, Tohoku University, Sendai 980-8577, Japan

Ken H. Andersen**
Institut Laue-Langevin, BP 156, F-38042, Grenoble Cedex 9, France
(March 18, 2000)

Magnetic diffuse scattering in the Zn-Mg-Ho icosahedral quasicrystal has been studied by neutron scattering over a wide $\boldsymbol{Q}$-range using a single-quasicrystalline sample. It was found that the diffuse scattering obeys the icosahedral symmetry, and appears as satellite peaks of the intense nuclear Bragg reflections. The diffuse-scattering patterns were successfully accounted for by assuming short-range spin correlations in a six-dimensional hypercubic crystal with a magnetic modulation vector $\boldsymbol{q} = (\frac{3}{4}, 0, 0, \frac{1}{2}, \frac{3}{4}, \frac{1}{2})_{\boldsymbol{a}^*}$. A possible origin for the six-dimensional spin correlations is discussed.

75.50.Kj, 75.50.Lk, 61.44.Br

I. INTRODUCTION

Since the discovery of quasicrystals [1–3], magnetic ordering of localized moments (spins) in quasiperiodic structures has been a fundamental issue of study. Theoretically, non-trivial magnetic orderings have been suggested for spin systems on ideal quasiperiodic structures [4–11]. On the other hand, experimental studies have been restricted to existing quasicrystals, which are mainly aluminum-transition-metal alloys. Some of those quasicrystals are *magnetic* [12–14]. However, the magnetic moments cannot be regarded as localized, since they originate from the itinerant d electrons of the transition-metal elements. Thus, it is not straightforward to elucidate the intrinsic nature of localized-spin systems in quasiperiodic structures from the experimental results.

Recently, icosahedral quasicrystals were discovered in the Zn-Mg-R system with R = rare-earth elements (rare-earth: RE = Gd, Tb, Dy, Ho or Er) and Y [15–17]. These quasicrystals are unique since they have well-localized and sizable 4f magnetic moments of the RE elements. Furthermore, X-ray structure analysis suggests that the RE elements are situated quasiperiodically at definite sites in the quasicrystals [18,19]. Thus, they provide an opportunity to study the behavior of localized spins in the quasiperiodic structure.

To date, the magnetism of the Zn-Mg-RE icosahedral quasicrystals has been studied by several groups. Exemplified by the RE = Ho system, the magnetic susceptibility shows a paramagnetic increase as temperature is decreased. It perfectly obeys the Curie-Weiss law at high temperatures [20–24]. The estimated effective moment is almost equal to that of a Ho^{3+} free ion. The magnetic susceptibility starts to deviate from the Curie-Weiss law below about 6 K [23]. The deviation is very small, suggesting a development of weak spin correlations and/or (quasi)crystalline-electric-field splitting. Then, it abruptly shows spin-glass-like freezing at $T_{\rm f} \sim 2$ K. The magnetic susceptibility of the other RE systems behaves quite similarly except for the difference in temperature scale. The spin-glass-like freezing was also detected in the temperature dependence of the ac susceptibility [22,24] and μSR relaxation rate [25].

Powder neutron diffraction was first performed by Charrier *et al.* [26]. They reported coexisting magnetic Bragg reflections and diffuse scattering, which simultaneously developed below $T_{\rm N}$, where $T_{\rm N} \simeq 7$ K for the Ho system. From this result, they concluded that magnetic long-range order is established below $T_{\rm N}$. However, long-range order is consistent neither with the susceptibility, nor with the μSR result. Indeed, two later studies revealed that high-quality icosahedral samples exhibit only the diffuse scattering part of the first work [27,28]. It was further suggested that the magnetic Bragg peaks, observed in the first work, can be attributed to crystalline contaminations [28]. Therefore, from the neutron powder diffraction and the susceptibility, one may conclude that the spins in the Zn-Mg-Ho icosahedral quasicrystal freeze below $T_{\rm f}$ with the static short-range spin correlations resulting in the magnetic diffuse scattering.

Since only short-range spin correlations are established, they are likely to reflect the intrinsic nature of the spin system in the Zn-Mg-Ho quasicrystal. Thus, detailed information on the spin correlations is highly desired. However,

the neutron powder diffraction experiments give only the spherical average of the magnetic scattering, so that the $\boldsymbol{Q}$-directional dependence of the spin correlations cannot be obtained. The aim of the present work is therefore to measure the diffuse scattering over a wide $\boldsymbol{Q}$-range using a single quasicrystal, and deduce characteristics of the associated short-range spin correlations. As a result, we have found that the diffuse scattering obeys the icosahedral symmetry. It appears quasiperiodically in $\boldsymbol{Q}$ space as satellite peaks of the intense nuclear Bragg reflections. The diffuse scattering patterns were analyzed by applying the section or projection method to the magnetic scattering [3,29–31]. We have successfully accounted for the diffuse-scattering patterns by assuming six-dimensional (6D) short-range spin correlations with modulation vector $\boldsymbol{q} = (\frac{3}{4}, 0, 0, \frac{1}{2}, \frac{3}{4}, \frac{1}{2})_{\boldsymbol{a}^*}$. The 6D short-range spin correlations is discussed in relation to the self-similarity, which is suggested to be inherent to the icosahedral quasicrystals.

The rest of the paper is organized as follows. The next section describes the experimental procedure. The results of the single-quasicrystal neutron scattering are presented in Sec. III, and are analyzed in Sec. IV. Discussion and conclusions are given in Sec. V. In Appendix A, definitions of coordinates in the scattering plane are given. Throughout this paper, we use notation and terminology that are specific to the section method. Thus, the section method is summarized in Appendix B. A part of this study has already been published in Ref. [28,32].

II. EXPERIMENTAL PROCEDURE

The 0.5 cm^3 single quasicrystal of $Zn_{60}Mg_{31}Ho_9$ was obtained by the Bridgman method from the incongruent melt of $Zn_{46}Mg_{51}Ho_3$. Details of the crystal growth were published elsewhere [33], while reports from other groups can be found in Refs. [34,35]. We note that the high perfection of the single quasicrystal was already confirmed by X-ray and neutron diffraction measurements in our previous reports [28,32,33].

The single quasicrystal was mounted in a standard ^{4}He refrigerator with its two-fold (2f), three-fold (3f) or five-fold (5f) axis vertical so that the scattering plane coincides with the 2f, 3f, or 5f plane, respectively. Unpolarized-neutron diffraction experiments were performed using the triple-axis spectrometer ISSP-GPTAS, and the multidetector diffractometer IMR-HERMES [36], installed at JRR-3M, JAERI (Tokai). The GPTAS was operated in the double-axis configuration, and collimations of 40'-80'-40' or 40'-80'-80' were employed. Incident neutrons of $k_{\rm i} \simeq 2.67$ Å^{-1} were selected by a vertically-focusing pyrolytic-graphite (PG) monochromator, and second harmonics was eliminated by a PG filter. For the HERMES diffractometer, incident neutrons of $k_{\rm i} = 3.45$ Å^{-1} were selected by a vertically-focusing germanium monochromator using 331 reflections. Higher order contamination is negligible for this diffractometer.

Polarized-neutron experiments were performed using the multidetector diffuse-scattering spectrometer D7 at the Institut Laue-Langevin (Grenoble) [37]. Incident neutrons of $k_i = 2.08$ Å^{-1} were selected by a vertically-focusing PG monochromator. Bender-type supermirrors were employed for the neutron polarization analysis. The nuclear-spin incoherent-scattering cross section is about 0.08 (barn/str FU) for the Zn-Mg-Ho icosahedral quasicrystal, which is quite small as compared with the magnetic scattering. (FU stands for the formula unit, and is defined as 1 FU = $Zn_6Mg_3Ho_1$.) Thus, instead of performing full XYZ polarization analysis, we measured spin-flip and non-spin-flip scattering with the neutron polarization direction aligned perpendicular to the scattering plane. The observed intensity was corrected for absorption and instrumental depolarization, and scaled to absolute units of cross section using a vanadium standard. Finally, the nuclear-spin incoherent scattering was subtracted numerically, and the spin-flip scattering is presented as the magnetic scattering. The main drawback of polarization analysis is the lower neutron intensity. This requires us to accumulate neutron counts for a long time in each position. Consequently, we could obtain data only sparsely in 3D reciprocal ($\boldsymbol{Q}_\parallel$) space: typically $\Delta|\boldsymbol{Q}_\parallel| \sim 0.2$ Å^{-1} for the 2θ direction, whereas for the ω direction, $|\Delta\boldsymbol{Q}_\parallel| \sim 0.2$ Å^{-1} at $|\boldsymbol{Q}_\parallel| \sim 2$ Å^{-1}.

III. RESULTS

A. Unpolarized neutron scattering

To obtain the overall features of the diffuse scattering over a wide $\boldsymbol{Q}$-range, we measured the scattering intensity for the 2f, 3f, and 5f planes using unpolarized neutrons. For the 2f plane, the triple-axis spectrometer GPTAS was used, whereas for the 3f and 5f planes, the experiments were carried out at the multidetector diffractometer HERMES. The measurements were made at two temperatures $T \simeq 1.3$ K and 20 K. Then, the magnetic scattering was deduced by the difference $I(T = 1.3\ {\rm K}) - I(T = 20\ {\rm K})$. This procedure will be justified in Sec. III B using polarized neutrons. We observed the magnetic scattering in a doubled symmetrically-independent-region in each plane, which will be shown

in Fig. 1 by solid lines. We confirmed that the magnetic scattering in the two independent regions is identical. (The icosahedral symmetry of the magnetic scattering will be further checked using the polarized neutron data.) The data were folded into a single independent region to increase the statistical precision and they were then unfolded to the full circle to improve the visibility of the symmetric features.

The magnetic-scattering-intensity maps are shown in Figs. 1(a), 1(b) and 1(c) for the 2f, 3f and 5f planes, respectively. Definitions of the (Q_H, Q_K) coordinates, used in the figures, are given in Appendix A. The positions of the intense nuclear Bragg reflections are also shown by white dots in the first quadrant of Fig. 1. As seen in the figures, the magnetic scattering is not spherical, but is highly structured with a number of spot-like peaks connected by weak diffuse-scattering ridges in all the planes. By comparing them with the Bragg positions, one can easily see that the diffuse scattering appears around the intense nuclear Bragg reflections. Thus, the short-range spin correlations are dominantly antiferromagnetic, which was first suggested from the magnetic susceptibility [20]. The spot-like peaks were examined in detail by performing several $\boldsymbol{Q}$ scans. As representative scans, we show the peak profiles around the $\boldsymbol{Q}_\parallel = (0, 0.55, 0)\text{Å}^{-1}$ along the $Q_{\parallel x}$ and $Q_{\parallel y}$ directions in Figs. 2(a) and 2(b), respectively. Clearly, the spots do not correspond to magnetic Bragg reflections, as evidenced by their finite widths. The correlation length was estimated from the widths as $\xi \sim 10$ Å in half width at half maximum (HWHM). In the 5f plane, the diffuse scattering around the origin appears like a continuous ring rather than spots (Fig. 1(c)). However, the ω-scan with fixed $|\boldsymbol{Q}_\parallel| = 0.55\text{Å}^{-1}$, shown in Fig. 3, clearly indicates peaks at every 36°, where $\boldsymbol{Q}_\parallel$ is along the 2f directions. Thus, the ring is a superposition of the ten diffuse peaks. Hence, the diffuse-scattering patterns can be regarded as consisting mainly of $\boldsymbol{Q}_\parallel$-localized diffuse peaks. This implies that the associated spin correlations are described by certain modulation vectors. The diffuse-scattering patterns will be analyzed and the modulation vector will be deduced in Sec. IV.

Shown in Fig. 4 is the temperature dependence of the peak intensity at $\boldsymbol{Q}_\parallel = (0.55, 0, 0)\text{Å}^{-1}$. The peak intensity evolves below $T_{\rm SRC} \simeq 5$ K, indicating that the spin correlations develop below this temperature. This almost corresponds to the beginning of the deviation in the susceptibility [23]. We note that $T_{\rm SRC}$ is considerably above $T_{\rm f}$. Hence, the spin correlations at $T_{\rm f} < T < T_{\rm SRC}$ are dynamic. The dynamic spin correlations can be observed so long as the spin dynamics is sufficiently slow, because in the double-axis experiments one observes an integrated scattering function for a certain energy range [38].

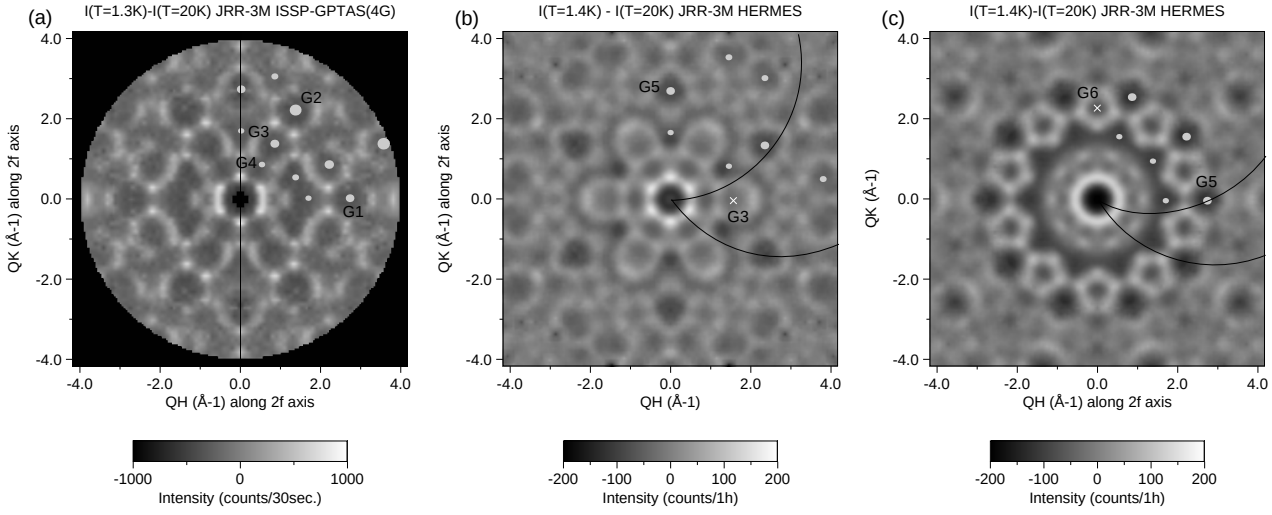

FIG. 1. Magnetic-scattering-intensity maps for the (a) 2f, (b) 3f, and (c) 5f planes. The magnetic scattering was deduced from the difference $I(T \simeq 1.4\text{K}) - I(T = 20\text{K})$. In the 2f plane, the two orthogonal axes of the scattering plane, Q_H and Q_K, are along the two orthogonal 2f axes. Whereas Q_K or Q_H is taken along the 2f axis for the 3f or 5f plane, respectively. For the (a) 2f plane, half of the plane, $Q_H > 0$, was measured, whereas for the (b) 3f or (c) 5f planes, observations were made only for the regions between the two solid lines. The white dots stand for the in-plane intense nuclear Bragg reflections in the first quadrant, while the white crosses stand for the projected positions of the out-of-plane Bragg reflections $\boldsymbol{G}_3$ and $\boldsymbol{G}_6$.

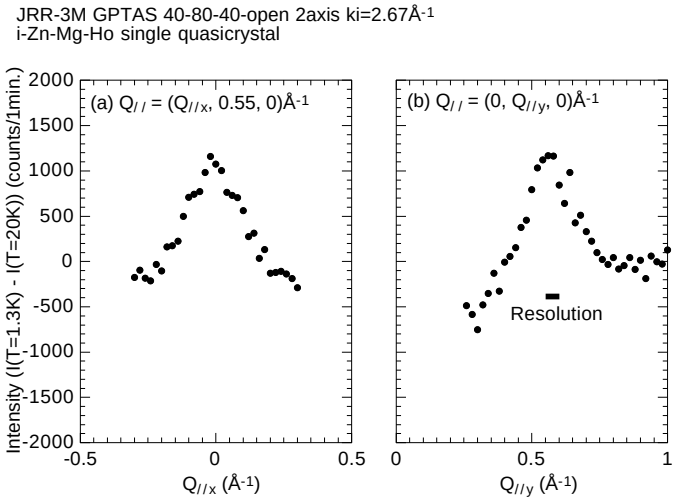

FIG. 2. Two $\boldsymbol{Q}$-scans around $\boldsymbol{Q}_{\parallel} = (0, 0.55, 0)$ along (a) the $Q_{\parallel x}$, and (b) the $Q_{\parallel y}$ directions. The magnetic scattering was deduced by the temperature difference $I(T = 1.3\text{K}) - I(T = 20\text{K})$.

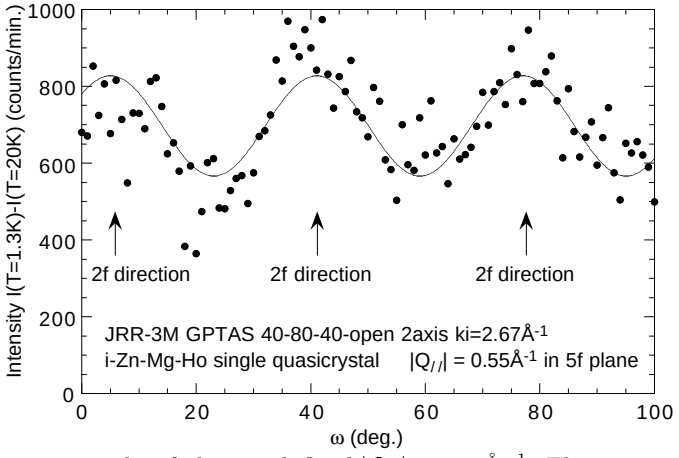

FIG. 3. An ω-scan around the origin in the 5f plane with fixed $|\boldsymbol{Q}_{\parallel}| = 0.55\text{Å}^{-1}$. The magnetic scattering was deduced by the difference $I(T = 1.3\text{K}) - I(T = 20\text{K})$. The 2f directions are shown by the arrows. Peaks can be seen along the 2f directions. The solid line is a sinusoidal guide to the eye.

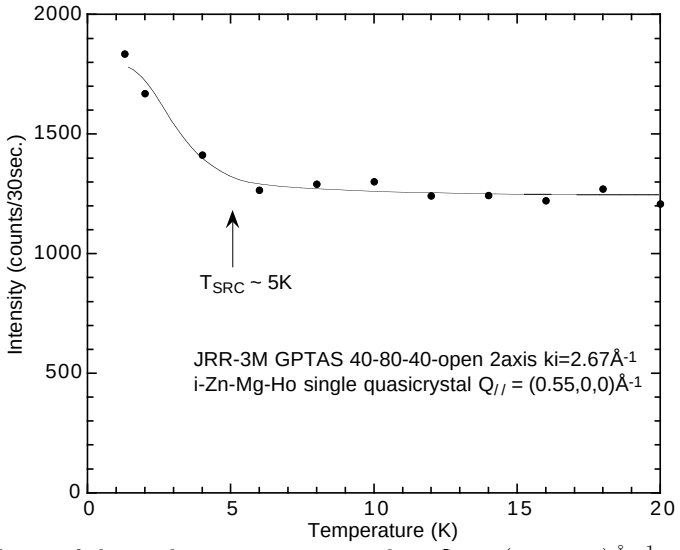

FIG. 4. Temperature dependence of the peak intensity measured at $\boldsymbol{Q}_{\parallel} = (0.55, 0, 0)\text{Å}^{-1}$ on the 2f axis. The peak evolves below $T_{\rm SRC} \sim 5$ K. The solid line is a guide to the eye.

B. Polarized neutron scattering

In the preceding subsection, we have deduced the magnetic scattering from the temperature difference. Since the observations were made at sufficiently low temperatures, i.e., $T \leq 20$ K, the nuclear scattering can reasonably be assumed as temperature-independent. Thus, the difference should at least show the development or temperature-variation of the magnetic scattering. However, to recognize the difference as the magnetic-scattering pattern at the lowest temperature, we have to confirm that the high-temperature reference data are paramagnetic and flat in the $\boldsymbol{Q}_{\parallel}$ space (except for the magnetic form factor). In addition, the difference cannot detect a paramagnetic-like background originating from randomly frozen spins at $T < T_{\rm f}$, because it has the same flat $\boldsymbol{Q}_{\parallel}$-dependence as the high temperature reference. Since randomly frozen spins are at the heart of the spin-glasses phenomena, the intensity of the paramagnetic-like background may contain essential information. We therefore performed a polarization analysis measurement, which can separate the magnetic scattering from the nuclear scattering without using a temperature difference. The resulting magnetic-scattering intensity is given in absolute units of cross-section, in the hope that it may be useful for further theoretical work.

The experiments were performed for the 2f plane at $T = 20$ K, and at $T = 1.6$ K for the 2f, 3f, and 5f planes. The sample was rotated over 360° to cover the full circle in the scattering plane, and the icosahedral symmetry of the magnetic scattering was confirmed in the raw data. We then folded and unfolded the data, similarly to the data treatment used for the unpolarized neutron scattering, in order to improve the statistical precision.

Shown in Fig. 5 is the magnetic-scattering-intensity map for the 2f plane observed at $T = 20$ K. The intensity map is almost structureless, and its $\boldsymbol{Q}_{\parallel}$-dependence is well described by the Ho^{3+} form factor [39]. This confirms that the system is paramagnetic at this temperature. Therefore, the temperature difference used in the preceding section does represent the magnetic scattering at low temperatures well, except for the paramagnetic-like background. The absolute value of the spin-flip scattering, extrapolated to $|\boldsymbol{Q}_{\parallel}| = 0$, is 2.7 (barn/str FU). This is in good agreement with the calculated paramagnetic scattering intensity, indicating the correctness of the procedure used to obtain the absolute intensity.

The intensity maps at $T \simeq 1.6$ K are shown in Figs. 6(a), 6(b), and 6(c) for the 2f, 3f and 5f planes, respectively. As compared with the unpolarized-neutron results in Fig. 1, fine structures are smeared out because of the large intervals of the observed $\boldsymbol{Q}_{\parallel}$-positions. However, the overall features, such as the positions of the intense peaks, are well reproduced. The maximum intensity, found around the origin, is about 3.5 (barn/str FU). Whereas the minimum is about 1.3 (barn/str FU) at $|\boldsymbol{Q}_{\parallel}| \sim 2.5\text{Å}^{-1}$, which, corrected for the form factor, corresponds to about 1.8 (barn/str FU) for $|\boldsymbol{Q}_{\parallel}| \to 0$. Thus, the peak intensity is almost twice the intensity of the paramagnetic-like background. This indicates that spin correlations develop quite significantly in the Zn-Mg-Ho quasicrystal.

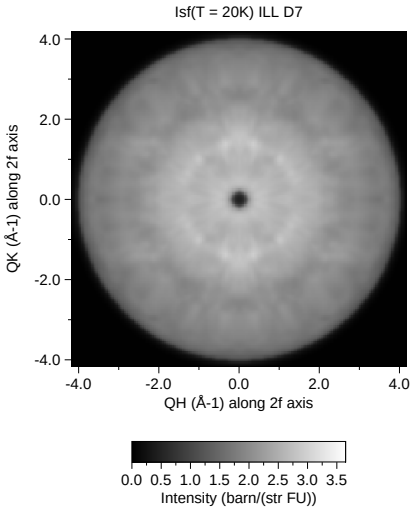

FIG. 5. A magnetic-scattering-intensity map at $T = 20$ K for the 2f plane obtained from the spin-flip scattering of polarized neutrons. The magnetic scattering is almost structureless, indicating that the system is paramagnetic at this temperature.

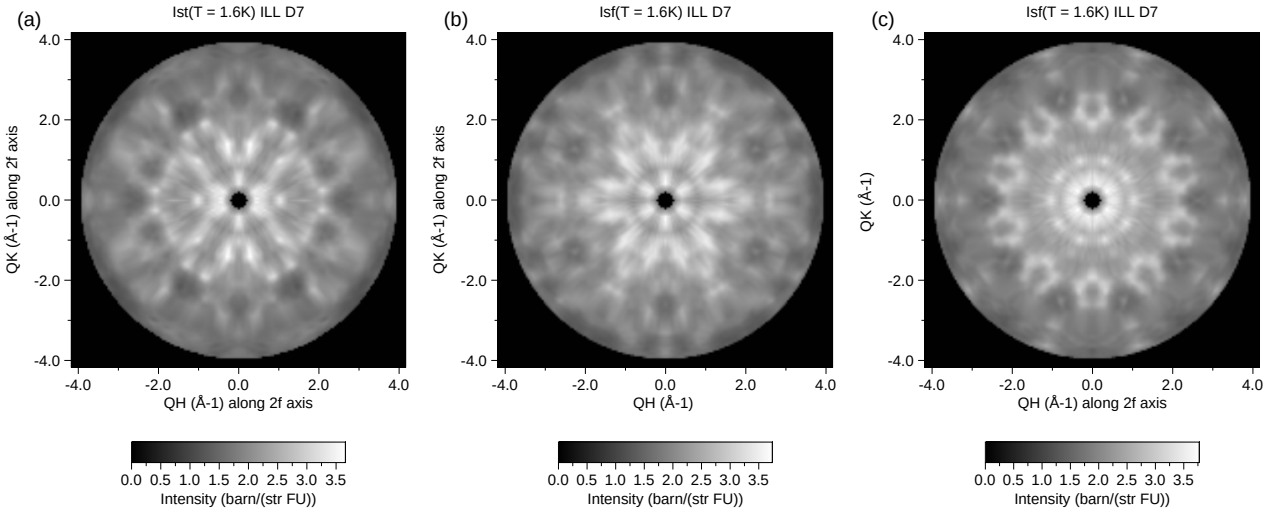

FIG. 6. Magnetic-scattering intensity maps at $T = 1.6$ K for the (a) 2f, (b) 3f and (c) 5f planes obtained from the spin-flip scattering of polarized neutrons. The peak intensity around the origin is about 3.5 (barn/str FU), whereas the minimum is 1.3 (barn/str FU) at $|\boldsymbol{Q}| \sim 2.5\text{Å}^{-1}$, where the square of the Ho^{3+} form factor is 0.73.

IV. ANALYSIS OF THE DIFFUSE-SCATTERING PATTERNS

A. Scattering intensity formula

Within the quasistatic approximation, the cross-sections of non-spin-flip ($\uparrow\uparrow$) and spin-flip ($\uparrow\downarrow$) scattering, observed in the double-axis experiments, are related to the instantaneous pair-correlation function of the magnetization operator $\hat{M}^{\alpha}(\boldsymbol{r}_{\parallel})$ ($\alpha = x, y, z$) as [40–42],

$$\left(\frac{\mathrm{d}\sigma}{\mathrm{d}\Omega}\right)_{\uparrow\uparrow} = (\gamma r_0)^2 \left(\frac{g_J}{2}\right)^2 \sum_{\alpha\beta} (e_{\parallel}^{\alpha} e_{\parallel}^{\beta}) < \hat{M}^{\alpha}(\boldsymbol{Q}_{\parallel}) \hat{M}^{\beta}(-\boldsymbol{Q}_{\parallel}) >, \tag{1}$$

$$\left(\frac{\mathrm{d}\sigma}{\mathrm{d}\Omega}\right)_{\uparrow\downarrow} = (\gamma r_0)^2 \left(\frac{g_J}{2}\right)^2 \sum_{\alpha\beta} (\delta_{\alpha,\beta} - (\tilde{Q}_{\parallel}^{\alpha} \tilde{Q}_{\parallel}^{\beta} + e_{\parallel}^{\alpha} e_{\parallel}^{\beta})) < \hat{M}^{\alpha}(\boldsymbol{Q}_{\parallel}) \hat{M}^{\beta}(-\boldsymbol{Q}_{\parallel}) >, \tag{2}$$

where,

$$< \hat{M}^{\alpha}(\boldsymbol{Q}_{\parallel}) \hat{M}^{\beta}(-\boldsymbol{Q}_{\parallel}) >= \int \mathrm{d}\boldsymbol{r}_{\parallel} \mathrm{d}\boldsymbol{r'}_{\parallel} \exp(-\mathrm{i}\boldsymbol{Q}_{\parallel} \cdot \boldsymbol{r}_{\parallel}) \exp(\mathrm{i}\boldsymbol{Q}_{\parallel} \cdot \boldsymbol{r'}_{\parallel}) < \hat{M}^{\alpha}(\boldsymbol{r}_{\parallel}) \hat{M}^{\beta}(\boldsymbol{r'}_{\parallel}) > . \tag{3}$$

γ, r_0 and g_J are the gyromagnetic ratio of the neutron, the classical electron radius, and the Landé g-factor, respectively. The unit vector along the scattering vector is denoted by $\tilde{\boldsymbol{Q}}_{\parallel}$, i.e., $\tilde{\boldsymbol{Q}}_{\parallel} = \boldsymbol{Q}_{\parallel}/|\boldsymbol{Q}_{\parallel}|$, while the up-spin direction of the neutrons is denoted by $\boldsymbol{e}_{\parallel}$. The experimental condition, $\boldsymbol{e}_{\parallel} \perp \boldsymbol{Q}_{\parallel}$, was used to derive the expressions [43]. The cross section for unpolarized neutrons is given as the sum of the two terms, Eqs. (1) and (2).

To construct a model pair-correlation function $< \hat{M}^{\alpha}(\boldsymbol{r}_{\parallel}) \hat{M}^{\beta}(\boldsymbol{r'}_{\parallel}) >$ that reproduces the observed scattering intensity, it is apparently necessary to perform the Fourier transform in Eq. (3) for arbitrary spin (or magnetization) correlations. However, because of the lack of the translational invariance, the Fourier transform in the 3D physical subspace is not straightforward, and can be performed only numerically. Fortunately, an icosahedral quasicrystal recovers the hidden translational symmetry in the 6D virtual space; it can be mapped on to a 6D periodic crystal by the section or projection method [3,29–31] (See also Appendix B for a summary of the section method). Indeed, the nuclear Bragg reflection intensity, necessary for the atomic structure analysis, is obtained with the aid of the higher-dimensional periodic crystal. We, here, apply the section method to the spin scattering and derive the cross-section formula for arbitrary spin correlations in the icosahedral quasicrystals.

In the section method, the atomic density of the periodic crystal in the virtual 6D space is assumed as Eq. (B1). Thus, one may write the spin density in the 6D virtual space, by replacing the atomic density of each Ho by its spin density, as,

$$\hat{M}^{\alpha}(\boldsymbol{r}) = \sum_{l,d} \hat{J}_{l,d}^{\alpha} \rho_s(\boldsymbol{r}_{\parallel} - (\boldsymbol{l}_{\parallel} + \boldsymbol{d}_{\parallel})) W(\boldsymbol{r}_{\perp} - (\boldsymbol{l}_{\perp} + \boldsymbol{d}_{\perp})), \tag{4}$$

where $\hat{J}_{l,d}^{\alpha}$ is the α-component of the virtual spin at the dth Ho site in the lth unit cell of the 6D crystal, and $\rho_s(\boldsymbol{r}_{\parallel})$ is defined so that $\hat{J}_{l,d}^{\alpha} \rho_s(\boldsymbol{r}_{\parallel} - (\boldsymbol{l}_{\parallel} + \boldsymbol{d}_{\parallel}))$ represents the spin density of a Ho^{3+} atom at $(\boldsymbol{l}_{\parallel} + \boldsymbol{d}_{\parallel})$ in the 3D physical subspace [44]. By definition, its Fourier transform, $f(\boldsymbol{Q}_{\parallel}) = \int \mathrm{d}\boldsymbol{r}_{\parallel} \exp(-\mathrm{i}\boldsymbol{Q}_{\parallel} \cdot \boldsymbol{r}_{\parallel}) \rho_s(\boldsymbol{r}_{\parallel})$, becomes the magnetic form factor. Since all Ho sites can be assumed to possess the same window functions [19], we neglect the d-dependence of $W_d(\boldsymbol{r}_{\perp})$. It is easy to confirm that the section at $\boldsymbol{r}_{\perp} = 0$ of the spin density, Eq. (4), represents the 3D array of the spins on the Ho sites in the quasicrystal, as,

$$\hat{M}^{\alpha}(\boldsymbol{r}_{\parallel}) = \hat{M}^{\alpha}(\boldsymbol{r}_{\parallel}, \boldsymbol{r}_{\perp} = 0) = \sum_{l,d} \hat{J}_{l,d}^{\alpha} \rho_s(\boldsymbol{r}_{\parallel} - (\boldsymbol{l}_{\parallel} + \boldsymbol{d}_{\parallel})) W(-(\boldsymbol{l}_{\perp} + \boldsymbol{d}_{\perp})). \tag{5}$$

Using Eq. (5), the pair correlation function in the 3D physical subspace can be written as,

$$\begin{aligned} < \hat{M}^{\alpha}(\boldsymbol{r}_{\parallel}) \hat{M}^{\beta}(\boldsymbol{r'}_{\parallel}) > \quad = \\ \sum_{l,d} \sum_{l',d'} < \hat{J}_{l,d}^{\alpha} \hat{J}_{l',d'}^{\beta} > \rho_s(\boldsymbol{r}_{\parallel} - \boldsymbol{l}_{\parallel} - \boldsymbol{d}_{\parallel}) \rho_s(\boldsymbol{r'}_{\parallel} - \boldsymbol{l'}_{\parallel} - \boldsymbol{d'}_{\parallel}) \\ \times W(-\boldsymbol{l}_{\perp} - \boldsymbol{d}_{\perp}) W(-\boldsymbol{l'}_{\perp} - \boldsymbol{d'}_{\perp}). \end{aligned} \tag{6}$$

Note that any spin correlations in the 3D physical subspace can be uniquely expressed by selecting appropriate $< \hat{J}_{l,d}^{\alpha} \hat{J}_{l',d'}^{\beta} >$. In fact, one can regard $< \hat{J}_{l,d}^{\alpha} \hat{J}_{l',d'}^{\beta} >$ as the correlation in the 3D physical subspace if only the atoms

which appear in the 3D physical subspace are concerned, while it can also be regarded as the 6D correlations if all the atoms are included. Thus, it is sufficient to find the 6D spin correlations that reproduce the observed scattering intensity.

Since the 6D crystal is periodic, it may possibly be easier to obtain the Fourier transform of the 6D spin correlations:

$$< \hat{J}^{\alpha}(\boldsymbol{Q})\hat{J}^{\beta}(-\boldsymbol{Q}) >= \sum_{\boldsymbol{l},\boldsymbol{d}} \sum_{\boldsymbol{l}',\boldsymbol{d}'} \exp(-\mathrm{i}\boldsymbol{Q}\cdot(\boldsymbol{l}+\boldsymbol{d}))\exp(\mathrm{i}\boldsymbol{Q}\cdot(\boldsymbol{l}'+\boldsymbol{d}'))< \hat{J}^{\alpha}_{l,d}\hat{J}^{\beta}_{l',d'} > . \tag{7}$$

On the other hand, using Eq. (6), we can relate $< \hat{M}^{\alpha}(\boldsymbol{Q})\hat{M}^{\beta}(-\boldsymbol{Q}) >$ to the 3D correlation function $< \hat{M}^{\alpha}(\boldsymbol{Q}_{\parallel})\hat{M}^{\beta}(-\boldsymbol{Q}_{\parallel}) >$ as,

$$\begin{aligned} &< \hat{M}^{\alpha}(\boldsymbol{Q}_{\parallel})\hat{M}^{\beta}(-\boldsymbol{Q}_{\parallel}) > \;\; = \\ &\qquad \frac{1}{(2\pi)^6}|f(\boldsymbol{Q}_{\parallel})|^2 \int \mathrm{d}\boldsymbol{Q}_{\perp}\mathrm{d}\boldsymbol{Q'}_{\perp} W(\boldsymbol{Q}_{\perp})W^{*}(\boldsymbol{Q'}_{\perp}) < \hat{J}^{\alpha}(\boldsymbol{Q}_{\parallel},\boldsymbol{Q}_{\perp})\hat{J}^{\beta}(-\boldsymbol{Q}_{\parallel},-\boldsymbol{Q'}_{\perp}) >, \end{aligned} \tag{8}$$

where $\hat{J}^{\alpha}(\boldsymbol{Q}) = \hat{J}^{\alpha}(\boldsymbol{Q}_{\parallel},\boldsymbol{Q}_{\perp})$ and $W(\boldsymbol{Q}_{\perp}) = \int \mathrm{d}\boldsymbol{r}_{\perp}\exp(-\mathrm{i}\boldsymbol{Q}_{\perp}\cdot\boldsymbol{r}_{\perp})W(-\boldsymbol{r}_{\perp})$ are used. If the correlation length in the 6D real space is sufficiently long, or in other words, if the diffuse peaks are well localized in the 6D $\boldsymbol{Q}$ space, $< \hat{J}^{\alpha}(\boldsymbol{Q}_{\parallel},\boldsymbol{Q}_{\perp})\hat{J}^{\beta}(-\boldsymbol{Q}_{\parallel},-\boldsymbol{Q'}_{\perp}) >$ may be negligibly small for $\boldsymbol{Q}_{\perp} \neq \boldsymbol{Q'}_{\perp}$. Then, Eq. (8) can be approximately written as,

$$< \hat{M}^{\alpha}(\boldsymbol{Q}_{\parallel})\hat{M}^{\beta}(-\boldsymbol{Q}_{\parallel}) > \simeq \frac{1}{(2\pi)^3}\frac{1}{V_{\perp}}|f(\boldsymbol{Q}_{\parallel})|^2 \int \mathrm{d}\boldsymbol{Q}_{\perp}|W(\boldsymbol{Q}_{\perp})|^2 < \hat{J}^{\alpha}(\boldsymbol{Q}_{\parallel},\boldsymbol{Q}_{\perp})\hat{J}^{\beta}(-\boldsymbol{Q}_{\parallel},-\boldsymbol{Q}_{\perp}) >, \tag{9}$$

where $V_{\perp}$ is the volume of the sample in the complementary subspace. Equation (9), together with Eqs. (1) and (2), shows that the 3D projection of $< \hat{J}^{\alpha}(\boldsymbol{Q})\hat{J}^{\beta}(-\boldsymbol{Q}) >$ gives the neutron scattering intensity. This is quite similar to the intensity of the nuclear Bragg reflections obtained in higher-dimensional crystallography.

We note that any spin correlations can also be directly expressed using the 3D pair-correlation $< \hat{M}^{\alpha}(\boldsymbol{Q}_{\parallel})\hat{M}^{\beta}(\boldsymbol{Q}_{\parallel}) >$, if we use, at most, an infinite number of $\vec{Q}_{\parallel}$ vectors in the 3D physical subspace. Nevertheless, we will use the 6D spin correlations in the following analysis, in the expectation that the observed magnetic scattering can be rather simply expressed by a small number of 6D modulation vectors.

B. Model spin correlations

As seen in the preceding subsection, it is sufficient to find 6D spin correlations that reproduce all the observations coherently. As the model 6D spin correlations, we assume most simply the following single-$\boldsymbol{q}$ spin correlations:

$$< \hat{\boldsymbol{J}}_{0,d}\cdot\hat{\boldsymbol{J}}_{l',d'} >_{\mathrm{A}} = J^2_{\mathrm{eff}}\cos\left(\boldsymbol{q}\cdot(\boldsymbol{d}-\boldsymbol{l}'-\boldsymbol{d}')\right)L\left(\boldsymbol{d}-\boldsymbol{l}'-\boldsymbol{d}'\right), \tag{10}$$

where J_{eff} is an effective spin defined as $g_J J_{\mathrm{eff}}\mu_{\mathrm{B}} = 10.6\mu_{\mathrm{B}}$. The subscript A indicates spatial average $< \hat{\boldsymbol{J}}_{0,d}\cdot\hat{\boldsymbol{J}}_{l',d'} >_{\mathrm{A}} = \frac{1}{N}\sum_m < \hat{\boldsymbol{J}}_{m,d}\cdot\hat{\boldsymbol{J}}_{m+l',d'} >$, where N is the number of unit cells [45]. The function $L(\boldsymbol{r})$ denotes a decay of the correlations, and obviously $L(0) = 1$. There are a number of microscopically different 6D spin correlations $< \hat{\boldsymbol{J}}_{l,d}\cdot\hat{\boldsymbol{J}}_{l',d'} >$ that give rise to the same average Eq. (10). They all give the same correlation function in the 6D reciprocal space as,

$$< \hat{\boldsymbol{J}}(\boldsymbol{Q})\cdot\hat{\boldsymbol{J}}(-\boldsymbol{Q}) >= \frac{1}{2}J^2_{\mathrm{eff}}N\frac{1}{v_0}\sum_{\boldsymbol{G}}|F_s(\boldsymbol{G})|^2\left(L(\boldsymbol{Q}-\boldsymbol{q}-\boldsymbol{G})+L(\boldsymbol{Q}+\boldsymbol{q}-\boldsymbol{G})\right), \tag{11}$$

where v_0 is the volume of the unit cell, and $L(\boldsymbol{Q})$ is defined as $L(\boldsymbol{Q}) = \int \mathrm{d}\boldsymbol{r}\exp(-\mathrm{i}\boldsymbol{Q}\cdot\boldsymbol{r})L(\boldsymbol{r})$. $F_s(\boldsymbol{G})$ denotes the structure factor for the Ho sites, defined by $F_s(\boldsymbol{G}) = \sum_d \exp(-\mathrm{i}\boldsymbol{G}\cdot\boldsymbol{d})$. Note that for sufficiently long-range correlations, Eq. (11) exhibits well-localized peaks at $\boldsymbol{Q} = \boldsymbol{G}\pm\boldsymbol{q}$ as satellites of the nuclear Bragg reflections.

Using Eqs. (1), (2), (9) and (11), one obtains the cross sections for the model spin correlations, Eq. (10), as,

$$\begin{aligned} \left(\frac{\mathrm{d}\sigma}{\mathrm{d}\Omega}\right) &= 2\left(\frac{\mathrm{d}\sigma}{\mathrm{d}\Omega}\right)_{(\uparrow\uparrow)} = 2\left(\frac{\mathrm{d}\sigma}{\mathrm{d}\Omega}\right)_{(\uparrow\downarrow)} \simeq \\ &\frac{1}{3}(\gamma r_0)^2\left(\frac{g_J J_{\mathrm{eff}}}{2}\right)^2|f(\boldsymbol{Q}_{\parallel})|^2\frac{N_{\mathrm{Ho}}}{(2\pi)^3 V_{\mathrm{w}}v_0} \\ &\times\sum_{\boldsymbol{G}}\int \mathrm{d}\boldsymbol{Q}_{\perp}|W(\boldsymbol{Q}_{\perp})|^2|F_s(\boldsymbol{G})|^2\left(L(\boldsymbol{Q}-\boldsymbol{q}-\boldsymbol{G})+L(\boldsymbol{Q}+\boldsymbol{q}-\boldsymbol{G})\right), \end{aligned} \tag{12}$$

where $N_{\rm Ho}$ and $V_{\rm w}$ are the number of the Ho atoms in the 3D icosahedral quasicrystal and the total volume of Ho windows in a 6D unit cell, respectively. To derive the above expression, we used the relation $< \hat{J}^x_{0,d}\hat{J}^x_{l',d'} >_{\rm A} = < \hat{J}^y_{0,d}\hat{J}^y_{l',d'} >_{\rm A} = < \hat{J}^z_{0,d}\hat{J}^z_{l',d'} >_{\rm A}$, because the spins are almost isotropic [22]. Furthermore, we neglected the non-diagonal terms for simplicity.

Equation (12) shows the characteristics of the neutron scattering intensity from the spin correlations in an icosahedral quasicrystal defined by the 6D single-$\boldsymbol{q}$ spin correlations. For sufficiently long-range correlations, diffuse-scattering peaks appear at $\boldsymbol{Q}_\parallel = \boldsymbol{G}_\parallel \pm \boldsymbol{q}_\parallel$ as satellite peaks of the nuclear Bragg reflections. The width of the peaks are given by the width of $L(\boldsymbol{Q})$ along the $\boldsymbol{Q}_\parallel$ directions. The intensity of the satellites is related to the complementary components of the 6D modulation vector, $\boldsymbol{q}_\perp$, through $|W(\boldsymbol{G}_\perp \pm \boldsymbol{q}_\perp)|^2$.

In the following subsections, we investigate the magnetic-scattering-intensity maps shown in Fig. 1. We try to find a possible candidate for $\boldsymbol{q}$ using a few of the main features of the observed diffuse-scattering-intensity maps. Then, we confirm that all the observed maps can be coherently explained by the 6D single-$\boldsymbol{q}$ spin correlations.

C. Physical-subspace components of the 6D modulation vectors

We first investigate the positions of the diffuse peaks around the origin $\boldsymbol{O}_\parallel$. As seen in Figs. 1(b) and 1(c), the diffuse peaks around $\boldsymbol{O}_\parallel$ appear on six and ten symmetrically-equivalent 2f-axes at $|\boldsymbol{Q}_\parallel| \simeq 0.55$Å^{-1} in the 3f and 5f planes, respectively. In the 2f plane, they also appear on the 2f-axes at $\boldsymbol{Q}_\parallel \simeq (0, \pm 0.55, 0)$Å^{-1} and $\boldsymbol{Q}_\parallel \simeq (\pm 0.55, 0, 0)$Å^{-1} as shown in Fig. 1(a). The diffuse peaks at $\boldsymbol{Q}_\parallel \simeq (\pm 0.55, 0, 0)$Å^{-1} are elongated along the Q_y (or Q_K) direction. Except for this, the diffuse-peak positions around $\boldsymbol{O}_\parallel$ are given by a set of symmetrically equivalent vectors $\{\boldsymbol{q}_\parallel\}$, where a representative $\boldsymbol{q}_\parallel = (0, 0.55, 0)$Å^{-1}. The elongated feature will be explained further below.

Next, we check the peak positions away from $\boldsymbol{O}_\parallel$. In the 2f plane, diffuse-scattering patterns similar to those around $\boldsymbol{O}_\parallel$ can be seen around the intense nuclear Bragg reflections, such as $\boldsymbol{G}_1 = (2, 4, 4, 0, -2, 0)_{\boldsymbol{a}^*}$, $\boldsymbol{G}_2 = (4, 2, 2, 2, 2, 2)_{\boldsymbol{a}^*}$ and $\boldsymbol{G}_3 = (3, 1, 1, 1, 1, 1)_{\boldsymbol{a}^*}$. In the 3f and 5f planes, the patterns around $\boldsymbol{O}_\parallel$ can be recognized around $\boldsymbol{G}_5 = (0, 2, -2, 4, 0, 4)_{\boldsymbol{a}^*}$. Thus, those diffuse peaks can possibly be regarded as satellites of the nuclear Bragg reflections, appearing at $\boldsymbol{Q}_\parallel = \boldsymbol{G}_\parallel + \{\boldsymbol{q}_\parallel\}$. The vertically elongated feature in the 2f plane mentioned above can be explained by superimposing satellites of other Bragg reflections on those of the origin. For instance, the $-\boldsymbol{q}_\parallel$ satellite of $\boldsymbol{G}_4 = (1, 1, 1, 1, 1, 1)_{\boldsymbol{a}^*}$ appears at $\boldsymbol{G}_{4\parallel} - (0, 0.55, 0) = (0.52, 0.29, 0)$Å^{-1}, which is on the elongated ridge. Note that additional different patterns appear in the 3f and 5f planes: at $|\boldsymbol{Q}| \sim 1.6$Å^{-1} in the 3f plane, circle-like patterns are seen, whereas pentagon-like patterns are seen at $|\boldsymbol{Q}| \sim 2.2$Å^{-1} in the 5f plane. They are fairly intense, and have no nuclear Bragg reflections at their centers in the 3f or 5f plane. Instead, they can be assigned to the intense Bragg reflections, $\boldsymbol{G}_3 = (3, 1, 1, 1, 1, 1)_{\boldsymbol{a}^*}$ and $\boldsymbol{G}_6 = (3, 3, 3, 1, -1, 1)_{\boldsymbol{a}^*}$, which are out of, but in vicinity of the planes. The projected positions of these out-of-plane Bragg reflections into the 3f and 5f planes are given by the white crosses in the figures. The positions coincide with the centers. Furthermore, the peak positions of these patterns can be found in the set of $\boldsymbol{G}_{3\parallel} + \{\boldsymbol{q}_\parallel\}$ or $\boldsymbol{G}_{6\parallel} + \{\boldsymbol{q}_\parallel\}$. These results suggest that all the peak positions can be described as the satellites of the intense nuclear Bragg reflections at $\boldsymbol{Q}_\parallel = \boldsymbol{G}_\parallel + \{\boldsymbol{q}_\parallel\}$. A possible candidate for $\boldsymbol{q}_\parallel$ is, then, $\boldsymbol{q}_\parallel = (0, 0.55, 0)$Å^{-1}. Since there are 15 2f-axes in the icosahedral symmetry, the number of the equivalent vectors is 30 by counting $\pm\boldsymbol{q}_\parallel$ independently. They most likely originate from short-range-ordered domains with symmetrically equivalent $\boldsymbol{q}_\parallel$, since these domains are in general equally populated. Hence, single-$\boldsymbol{q}$ correlations can plausibly be realized in each domain.

D. A possible modulation vector in the 6D reciprocal space

The most prominent feature in the observation is the different intensities of the $\pm\boldsymbol{q}_\parallel$ satellites of the Bragg reflections. For example, one can see substantially different intensities for the $\pm(0, 0.55, 0)$Å^{-1} satellites of $\boldsymbol{G}_2$ or $\boldsymbol{G}_3$. In the 6D reciprocal space, the $\pm\boldsymbol{q}$ satellite-peaks have the same intensity, as seen Eq. (11). Thus, the difference in intensity indicates that $\boldsymbol{q}_\perp \neq 0$, since in this case $|W(\boldsymbol{G}_\perp + \boldsymbol{q}_\perp)|^2$ can differ from $|W(\boldsymbol{G}_\perp - \boldsymbol{q}_\perp)|^2$ in Eq. (12). On the other hand, the satellites around the origin, $\boldsymbol{O}_\parallel + \{\boldsymbol{q}_\parallel\}$, appear most intensely in the observation. Since $|W(\boldsymbol{Q}_\perp)|^2$ is a rapidly decreasing function of $|\boldsymbol{Q}_\perp|$ in general, a peak with small $|\boldsymbol{Q}_\perp|$ can have high intensity. Thus, $\boldsymbol{O}_\perp + \{\boldsymbol{q}_\perp\}$ $(= \{\boldsymbol{q}_\perp\})$ should be small, otherwise, a satellite of another reflection may have a smaller $|\boldsymbol{Q}_\perp|$, and may appear as a more intense peak. Hence, together with $\boldsymbol{q}_\parallel$ deduced before, the $\boldsymbol{q}$ vector should be $\boldsymbol{q} = (\boldsymbol{q}_\parallel, \boldsymbol{q}_\perp) \simeq (0, 0.55, 0, \delta_4, \delta_5, \delta_6)$Å^{-1}, where $\delta_n \sim 0$ and $\sum_n |\delta_n| \neq 0$ for $n = 4, 5, 6$. By restricting the modulation to be commensurate to the 6D periodic crystal,

we find the simplest vector that satisfies the above as $(\frac{3}{4},0,0,\frac{1}{2},\frac{3}{4},\frac{1}{2})_{\boldsymbol{a}^*}(\simeq (0,0.547,0,0,0.019,0)\text{Å}^{-1})$ with the 6D reciprocal-lattice basis.

E. Scattering intensity from the 6D spin correlations

We, here, calculate the scattering intensity of all the satellites for the 6D single-$\boldsymbol{q}$ spin correlations with $\boldsymbol{q} = (\frac{3}{4},0,0,\frac{1}{2},\frac{3}{4},\frac{1}{2})_{\boldsymbol{a}^*}$ using Eq. (12). For the calculation, it is necessary to assume a trial function for $L(\boldsymbol{r})$. Since we intend to reproduce only the overall features of the scattering intensity, but not to discuss the peak shapes, any function that reproduces the observed correlation length $\xi \sim 10$Å can be used. Thus, we use the following mathematically-simplest trial function [46]:

$$L(\boldsymbol{r}) = \exp\left(-\kappa^2|\boldsymbol{r}|^2 \ln 2\right), \tag{13}$$

where $\kappa \sim 0.1\text{Å}^{-1}$ is the inverse of ξ. Note that $L(\boldsymbol{r})$ is isotropic in the 6D space, i.e., κ is independent of direction. We use the window function and positions of the Ho atoms proposed by Ohno and Ishimasa [19]. In short, the window is spherical, and has a double-shell structure for Ho sites: $W(\boldsymbol{r}_\perp) = 1$ for $5.5\text{Å} < |\boldsymbol{r}_\perp| < 7.8\text{Å}$, otherwise $W(\boldsymbol{r}_\perp) = 0$. The Ho atoms are at $\boldsymbol{d} = \frac{1}{4}(3,1,1,1,1,1)_{\boldsymbol{a}^*}$ and equivalent positions, in the unit cell. See Ref. [19] for details. Satellite diffuse peaks from 4327 nuclear Bragg reflections $\boldsymbol{G}$ were taken into account, where the Bragg reflections were selected by the condition $|\boldsymbol{G}_\perp| < 0.6\text{Å}^{-1}$. The integration in Eq. (12) was performed numerically for several integration steps to obtain optimum conditions. The resulting intensity was averaged for the short-range-ordered domains with 30 equivalent $\boldsymbol{q}$-vectors.

The calculated intensity maps are shown in Figs. 7(a-c). They are given in absolute units of spin-flip scattering. As seen by comparing the results with Fig. 1, the symmetry and relative intensity of the diffuse scattering are well reproduced by the calculation. In the 2f plane, the intensity ratio of satellite peaks, such as at $\boldsymbol{G}_{3\parallel} \pm (0,0.55,0)\text{Å}^{-1}$ or at $\boldsymbol{G}_{2\parallel} \pm (0,0.55,0)\text{Å}^{-1}$, is in good agreement with the experimental results. The vertically elongated feature at $\boldsymbol{Q}_\parallel = (\pm 0.55,0,0)\text{Å}^{-1}$ is also fairly well reproduced. For the 3f and 5f planes, circle-like and pentagon-like patterns can be seen in the calculations, which agree well with the experimental data. In addition, the weak diffuse-scattering ridges connecting the spot-like peaks, such as those running parallel to the 5f axes in the 2f plane, are well reproduced in the calculation, indicating that they consist of many weak $\boldsymbol{q}$-localized peaks. The good correspondence between observation and calculation strongly confirms the validity of the 6D magnetic modulation vector. Hence, the spin correlations in the 3D icosahedral quasicrystal can be regarded as the projection of the 6D spin correlations with the modulation vector $\boldsymbol{q} = (\frac{3}{4},0,0,\frac{1}{2},\frac{3}{4},\frac{1}{2})_{\boldsymbol{a}^*}$. The vector indicates that the diffuse scattering appears where the nuclear Bragg reflections are absent, and thus the corresponding spin correlations can be regarded as antiferromagnetic in the 6D virtual space.

As concerns the absolute intensity, one finds slightly lower peak intensities in the calculation in comparison to the polarization-analysis results in Fig. 6. The difference is about 1 (barn/ str FU). This may originate from small but finite $< \hat{J}^\alpha(\boldsymbol{Q}_\parallel,\boldsymbol{Q}_\perp)\hat{J}^\beta(\boldsymbol{Q}_\parallel,\boldsymbol{Q'}_\perp) >$ for $\alpha \neq \beta$ and $\boldsymbol{Q}_\perp = \boldsymbol{Q'}_\perp$, or for $\alpha = \beta$ and $\boldsymbol{Q}_\perp \neq \boldsymbol{Q'}_\perp$, which is assumed to be negligible in Eq. (12) or Eq. (9), respectively. In addition, the paramagnetic-like background is absent in the calculation, because we did not take into account the randomly frozen spins, which may exist in the Zn-Mg-Ho icosahedral quasicrystal. Except for these minor discrepancies, we may conclude that the model spin correlations, given in Eq. (10), reproduce the observation in a semi-quantitative manner. We note that the qualitative features, such as the intensity ratio of the satellite peaks, are unchanged for small variations in the window functions. However, it may possibly affect the results quantitatively. Thus, for further quantitative discussion, precise determination of window functions and window positions may be necessary. The single-quasicrystal structure analysis is now in progress [47].

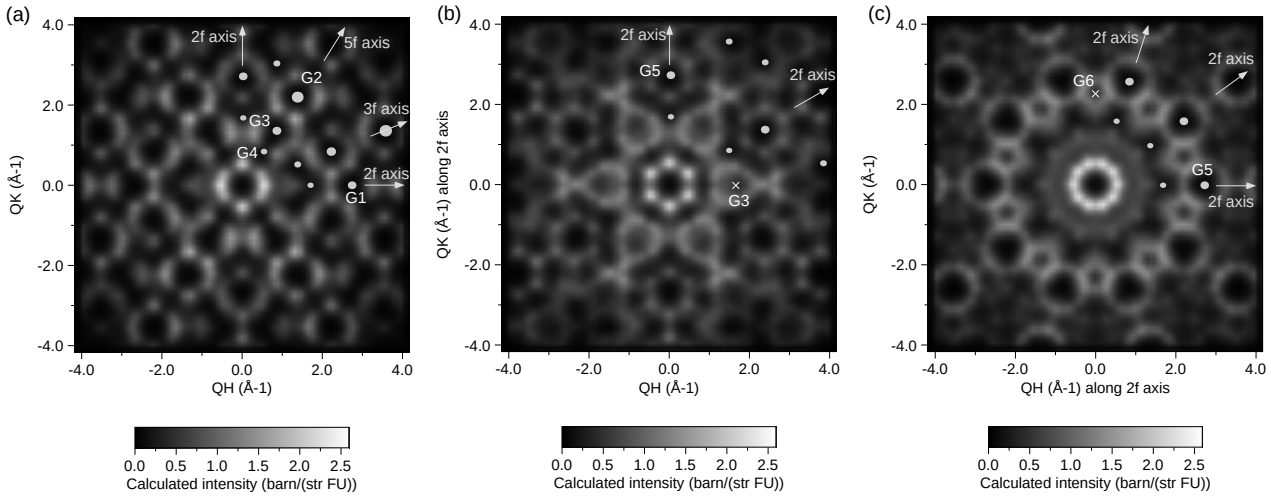

FIG. 7. Calculated intensity of the magnetic diffuse scattering for the (a) 2f, (b) 3f, and (c) 5f planes. The white dots stand for the in-plane intense nuclear Bragg reflections, while the white crosses stand for the projected positions of the out-of-plane Bragg reflections $\boldsymbol{G}_3$ and $\boldsymbol{G}_6$.

V. DISCUSSION AND CONCLUSIONS

In the present study, the magnetic diffuse scattering in the Zn-Mg-Ho icosahedral single quasicrystal has been intensively investigated by neutron scattering. It has been found that the diffuse-scattering patterns can be explained by assuming short-range spin correlations that are given as the section of the single-$\boldsymbol{q}$ correlations in the 6D periodic crystal with $\boldsymbol{q} = (\frac{3}{4}, 0, 0, \frac{1}{2}, \frac{3}{4}, \frac{1}{2})_{\boldsymbol{a}^*}$. Why are the spin correlations expressed by the single 6D modulation vector rather than by a 3D modulation vector? It has been suggested that the Ho atoms are quasiperiodically situated in the icosahedral quasicrystal [19,18]. Consequently, the spin Hamiltonian cannot be translationally invariant, and thus cannot be diagonalized in 3D $\boldsymbol{Q}_{\parallel}$-space. Hence, it may be reasonable that the spin-correlations are not described by a 3D modulation vector. However, since the 6D space is virtual space, it seems unlikely that the spin Hamiltonian is defined in the 6D space [48]. We, here, try to give a crude explanation for the origin of 6D spin correlations using an analogy to the 1D quasicrystal, i.e., the Fibonacci lattice.

As shown in Fig. 8(a), the 1D quasicrystal is given by the section of the 2D square lattice consisting of atoms elongated along the complementary subspace ($r_{\perp}$). The quasicrystal structure has remarkable self-similarity or local isomorphism, which ensures that an arbitrary atomic structure of size r can be found at a distance of about $2r$. Assume that spin correlations are established in a region where the spins are rather densely situated (or a region favorable for other reasons). Then, it is natural that the same correlations develop in same atomic-structure regions, which can be found anywhere in the quasicrystal (lower panel of Fig. 8(b)). The same structure regions are the section (or projection) of the same structure units in the 2D space, and thus, one sees the same spin correlations developing around the physical subspace ($r_{\parallel}$) in the 2D virtual space (Upper panel of Fig. 8(b)). Then, one may extend the spin correlations in all the 2D virtual space, so that the 1D section of the correlations corresponds to the real spin correlations in the physical subspace (Fig. 8(c)). It is easy to find that the resulting 2D spin correlations are expressed by a single 2D modulation vector. Although the atomic structure specific to the Zn-Mg-Ho icosahedral quasicrystal has not yet been determined completely, it is widely believed that self-similarity holds in real icosahedral quasicrystals [49]. Thus, it appears plausible that this 1D analogy can explain the observed 6D single-$\boldsymbol{q}$ short-range spin correlations.

The above argument implicitly infers that the correlation length becomes infinitely large at the lowest temperature, since there is no upper limit in r at which the self-similarity breaks, except for the trivial sample size. However, as observed in the experiments, the development of the spin correlations terminates with a somewhat short correlation

length of $\xi \sim 10$Å(HWHM). The origin of this spin freezing may be as follows. As suggested in the X-ray structure analysis, there can be fluctuation of Zn and Mg for certain atomic sites in 6D periodic crystal [19]. This can produce a random (quasi)crystalline-electric-field around each Ho^{3+} ion, which results in random anisotropy. Hence, at a certain temperature lower than the anisotropy energy, spin-glass-like freezing may take place, as seen in the random-magnetic-anisotropy model [50,51]. The random anisotropy should be small, because the magnetic susceptibility shows a Curie-Weiss behavior above ~ 5 K with the effective moment equal to that of the free Ho^{3+} ion. This is consistent with the low freezing temperature $T_{\rm f} \sim 2$ K.

Although this seems quite plausible as an origin of the freezing, there may be another possibility. Recently, a Monte Carlo study was performed for Ising spins on the Zn-Mg-Ho model structure by Matsuo *et al.* [52]. They do not introduce any randomness in the local anisotropy nor spin-spin interactions. Nevertheless, a short-range-ordered state was obtained at $T \simeq 0$ K, where spin fluctuations are suppressed, for a certain set of exchange interactions. Jagannathan and Schulz studied the Hubbard model for electrons in two-dimensional quasiperiodic (octagonal) tiling [53]. At the half-filling, where the $U \to \infty$ limit gives an antiferromagnetic Heisenberg Hamiltonian, the model shows self-similar (possibly short-range) magnetic correlations. In view of these theoretical results, it may be possible that the spin freezing is an intrinsic property of quasiperiodic spin systems, and unrelated to randomness. To elucidate the origin of the spin-freezing behavior, further theoretical work seems to be necessary, not only on the short-range ordered ground-state, but also on the ordering process at finite temperatures. In addition, neutron inelastic-scattering may help to distinguish whether the system behaves similarly to ordinary spin-glasses or not, because it can give the temperature dependence of the relaxation time. Such experiments are now in progress.

Despite the observed short correlation length, it may be worthwhile examining the long-range-order limit of the single-$\boldsymbol{q}$ 6D spin correlations. In this limit, the 6D periodic crystal is magnetically decomposed into sublattices, whose unit cells are 64 times larger than the original unit cell. Each sublattice is projected into the 3D physical subspace as an interpenetrating quasiperiodic structure, where all the spins point in the same direction. Consequently, along any straight line in the 3D physical subspace, the sequence of the spin direction is quasiperiodic. Hence, one can say that the 6D long-range correlations correspond to the quasiperiodic spin configuration in the 3D physical subspace. Thus, the observed short-range spin correlations have the quite unique characteristic that they become *quasiperiodic* spin correlations in the long-range-order limit.

In view of the short correlation length, one may think that the spin correlations develop in atomic clusters, since there is general agreement on the existence of clusters with a diameter of ~ 10Å (corresponding to a full width) for the Al-TM icosahedral quasicrystal [54]. However, so far no clusters with such a large diameter have been found in the Zn-Mg-RE quasicrystal, instead, a recent report suggests the absence of such clusters [55]. Thus, the possibility can be discounted for the present moment. We note that even if such a cluster model is constructed in the future, the spin configuration in the cluster can be easily inferred from the present $\boldsymbol{q}$ vector, with the help of the 6D crystallography.

Finally, a comment on our previous report [28]. In the report, we suggested the presence of quasi-five-dimensional (Q5D) spin-correlations solely from the weak diffuse-scattering ridges running parallel to the 5f axis in the 2f plane. However, we have found that the Q5D spin-correlations cannot explain the magnetic diffuse-scattering patterns in the 3f and 5f planes. In the present work, we have regarded the diffuse scattering as a set of satellite peaks described by the $\boldsymbol{q}$-localized modulation vector. The intensity calculation, performed with an isotropic correlation length, reproduces the observation semi-quantitatively. This indicates that the spin correlations are rather 6D than Q5D. The origin of the diffuse ridges can be understood as follows; along the 5f axis there are a number of Bragg reflections that have relatively small $\boldsymbol{G}_{\perp}$, and thus their satellites are observable almost continuously.

In conclusion, a detailed neutron-scattering study has been performed on the Zn-Mg-Ho icosahedral single quasicrystal. We have measured the magnetic diffuse-scattering over a wide $\boldsymbol{Q}$-range in the 2f, 3f, and 5f planes. It was found that the diffuse scattering appears as satellites of the intense nuclear Bragg reflections. The diffuse-scattering patterns are successfully accounted for by assuming 6D single-$\boldsymbol{q}$ spin correlations with the modulation vector $\boldsymbol{q} = (\frac{3}{4}, 0, 0, \frac{1}{2}, \frac{3}{4}, \frac{1}{2})_{\boldsymbol{a}^*}$. A possible origin of the 6D spin correlations is discussed in terms of the self-similarity, which may be an inherent property of icosahedral quasicrystals.

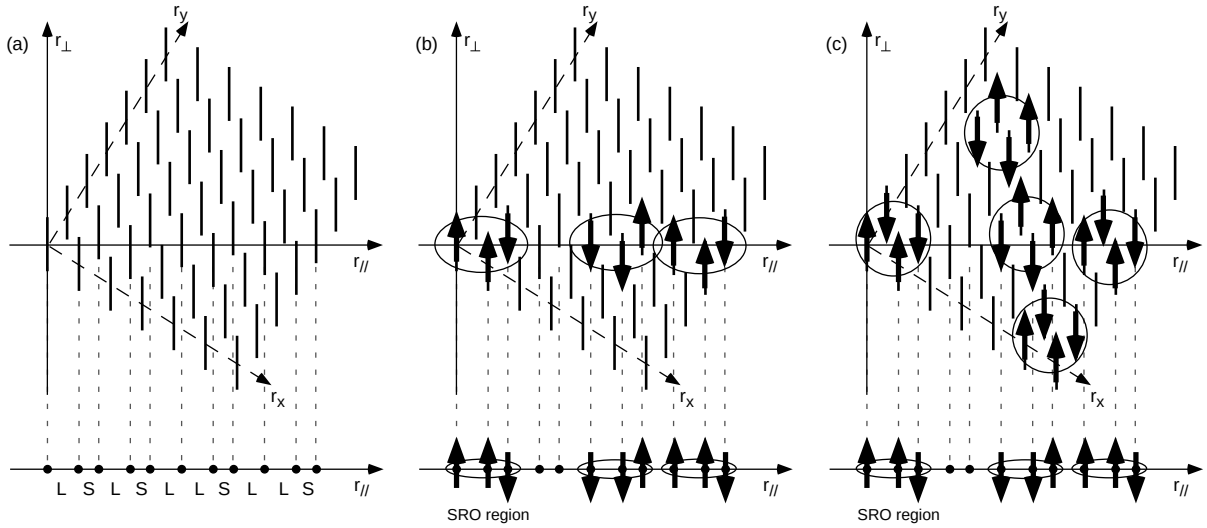

FIG. 8. (a) Schematic illustration of a 1D quasicrystal obtained as a section of a 2D square lattice. (b) (Lower panel) the spin correlations in small regions denoted by "SRO region", and (upper panel) corresponding spin correlations in the 2D square lattice defined only between the spins on the 1D section. For $T > T_{\rm f}$ the figure should be regarded as a *snap-shot* in time, whereas $T < T_{\rm f}$ the correlations become static. (c) (Lower panel) same as the lower panel of (b). (Upper panel) the virtual spin correlations extended to the 2D space. The $\boldsymbol{q}$ vector for this correlations is $\pm(0, 0.5)$. Note that only when both of the spins are on the 1D section, the spin correlation function is projected, as seen in Eq. (6). Thus, the correlations shown in (b) and (c) are essentially identical for the intensity-calculation purpose.

VI. ACKNOWLEDGEMENTS

The present authors thank Drs. E. Abe, L. H. Tang, I. R. Fisher, A. Mishchenko and S. Matsuo for valuable discussions, and Drs. T. Ishimasa and B. Charrier for providing us with their results prior to publication. They also thank NSL, ISSP, University of Tokyo, and Institut Laue-Langevin for assistance in the neutron scattering experiments. The numerical integration in Sec. IV was performed using the SX-4 supercomputer at National Research Institute for Metals.

APPENDIX A: COORDINATES IN THE SCATTERING PLANES

In the experiments, the 2f, 3f and 5f planes in the 3D physical-subspace are chosen as the scattering planes. We specify a position in each scattering plane by (Q_H, Q_K), using two orthogonal basis vectors defined in the plane. The position (Q_H, Q_K) corresponds to $\boldsymbol{Q}_{\parallel}$ as: (i) $\boldsymbol{Q}_{\parallel} = (Q_H, Q_K, 0)$ for the 2f plane; (ii) $\boldsymbol{Q}_{\parallel} = (\frac{1}{\sqrt{3}\tau}Q_H, \frac{\tau}{\sqrt{3}}Q_H, Q_K)$ for the 3f plane; (iii) $\boldsymbol{Q}_{\parallel} = (\frac{\tau}{\sqrt{1+\tau^2}}Q_K, \frac{1}{\sqrt{1+\tau^2}}Q_K, Q_H)$ for the 5f plane.

APPENDIX B: SUMMARY OF THE SECTION METHOD

The icosahedral quasicrystal is related to a 6D periodic crystal by the section or projection method [3,29–31]. In this appendix, we summarize the section method to define notations, terminology and coordinates.

Six-dimensional real space, where the 6D periodic crystal is defined, is spanned by six orthogonal unit basis vectors $\boldsymbol{x}_1, ..., \boldsymbol{x}_6$. The basis vectors are chosen so that the first three vectors, $\boldsymbol{x}_1, ..., \boldsymbol{x}_3$, coincide with the basis vectors of the 3D physical (external or parallel) subspace, i.e., $\boldsymbol{x}, \boldsymbol{y}, \boldsymbol{z}$. On the other hand, $\boldsymbol{x}_4, ..., \boldsymbol{x}_6$ span the 3D complementary

(internal or perpendicular) subspace. A position in the 6D real space is written as $\boldsymbol{r} = \sum_{i=1}^{6} r_i \boldsymbol{x}_i = (r_1, ..., r_6) = (\boldsymbol{r}_\parallel, \boldsymbol{r}_\perp)$, where $\boldsymbol{r}_\parallel = \sum_{i=1}^{3} r_i \boldsymbol{x}_i = (r_1, r_2, r_3)$ stands for the projected position of $\boldsymbol{r}$ into the physical subspace, whereas $\boldsymbol{r}_\perp = \sum_{i=4}^{6} r_i \boldsymbol{x}_i = (r_4, r_5, r_6)$ for the position into the complementary subspace. In reciprocal space, a $\boldsymbol{Q}$-vector is defined similarly as $\boldsymbol{Q} = \sum_{i=1}^{6} Q_i \boldsymbol{x}_i = (Q_1, ..., Q_6) = (\boldsymbol{Q}_\parallel, \boldsymbol{Q}_\perp)$.

The basis vectors of the 6D periodic crystal are given as $\boldsymbol{a}_1 = \alpha(1, \tau, 0, \tau, -1, 0)$, $\boldsymbol{a}_2 = \alpha(\tau, 0, 1, -1, 0, \tau)$, $\boldsymbol{a}_3 = (\tau, 0, -1, -1, 0, -\tau)$, $\boldsymbol{a}_4 = \alpha(0, 1, -\tau, 0, \tau, 1)$, $\boldsymbol{a}_5 = (-1, \tau, 0, -\tau, -1, 0)$, and $\boldsymbol{a}_6 = \alpha(0, 1, \tau, 0, \tau, -1)$, where τ is the golden ratio and $\alpha = a/\sqrt{2+\tau}$ [56]. The 6D lattice constant is given by $a_{6\mathrm{D}} = \sqrt{2}a$. The lattice vectors, $\boldsymbol{l}$, are given by $\boldsymbol{l}(= (l_1, ..., l_6) = (\boldsymbol{l}_\parallel, \boldsymbol{l}_\perp)) = \sum_{i=1}^{6} l_i' \boldsymbol{a}_i = (l_1', ..., l_6')_{\boldsymbol{a}}$, where l_i' are integers. Subscript $\boldsymbol{a}$ indicates that the vector is defined with the $\boldsymbol{a}_i$-vector basis. The above basis vectors are chosen so that the three orthogonal 2f-axes of the icosahedral symmetry coincide with the three principle axes in the physical subspace, namely $\boldsymbol{x}_1, \boldsymbol{x}_2, \boldsymbol{x}_3$ [56].

Since the 6D crystal is periodic, we can define a reciprocal lattice; basis vectors of the reciprocal lattice are $\boldsymbol{a}_i^* = \boldsymbol{a}_i/(2a^2)$. Reciprocal-lattice vectors are then given by $\boldsymbol{G}(= (G_1, ..., G_6) = (\boldsymbol{G}_\parallel, \boldsymbol{G}_\perp)) = \sum_{i=1}^{6} G_i' \boldsymbol{a}_i^* = (G_1', ..., G_6')_{\boldsymbol{a}^*}$ with the G_i' being integers. The subscript $\boldsymbol{a}^*$ is used to indicate that the basis vectors are $\boldsymbol{a}_i^*$.

Suppose that there are several atoms in a unit cell of the 6D periodic crystal, which are not necessarily the same elements. Then, the position of the dth atom in the lth cell is given by $\boldsymbol{l} + \boldsymbol{d}$, where $\boldsymbol{d} = \sum_{i=1}^{6} d_i' \boldsymbol{a}_i$ with $0 \le d_i' < 1$. The dth atom spreads over a region Ω_d, called an occupation or acceptance domain, in the complementary subspace, whereas in the physical subspace it has an atomic density $\rho_d(\boldsymbol{r}_\parallel)$. Thus, the total atomic density in the 6D space is written as,

$$\rho(\boldsymbol{r}) = \sum_{l,d} \rho_d(\boldsymbol{r}_\parallel - (\boldsymbol{l}_\parallel + \boldsymbol{d}_\parallel)) W_d(\boldsymbol{r}_\perp - (\boldsymbol{l}_\perp + \boldsymbol{d}_\perp)), \tag{B1}$$

where the window function $W_d(\boldsymbol{r}_\perp)$ represents the shape of Ω_d as,

$$W_d(\boldsymbol{r}_\perp) = \begin{cases} 1, \boldsymbol{r}_\perp \in \Omega_d \\ 0, \text{otherwise.} \end{cases} \tag{B2}$$

The atomic density in the 3D physical-subspace is given by the section of the 6D periodic crystal at $\boldsymbol{r}_\perp = 0$ as

$$\rho(\boldsymbol{r}_\parallel) = \rho(\boldsymbol{r}_\parallel, \boldsymbol{r}_\perp = 0) = \int \mathrm{d}\boldsymbol{r}_\perp \rho(\boldsymbol{r}_\parallel, \boldsymbol{r}_\perp) \delta(\boldsymbol{r}_\perp) = \sum_{l,d} \rho_d(\boldsymbol{r}_\parallel - (\boldsymbol{l}_\parallel + \boldsymbol{d}_\parallel)) W_d(-(\boldsymbol{l}_\perp + \boldsymbol{d}_\perp)) \tag{B3}$$

Nuclear scattering is related to $|\rho(\boldsymbol{Q}_\parallel)|^2$, where $\rho(\boldsymbol{Q}_\parallel)$ is the Fourier transform of $\rho(\boldsymbol{r}_\parallel)$, defined as $\rho(\boldsymbol{Q}_\parallel) = \int \mathrm{d}\boldsymbol{r}_\parallel \exp(-\mathrm{i}\boldsymbol{Q}_\parallel \cdot \boldsymbol{r}_\parallel) \rho(\boldsymbol{r}_\parallel)$. From Eq. (B3), one can immediately obtain,

$$|\rho(\boldsymbol{Q}_\parallel)|^2 \propto \sum_{\boldsymbol{G}} \int \mathrm{d}\boldsymbol{Q}_\perp |F(\boldsymbol{Q})|^2 \delta(\boldsymbol{G} - \boldsymbol{Q}), \tag{B4}$$

where the structure factor $F(\boldsymbol{Q})$ is defined as $F(\boldsymbol{Q}) = \sum_d \exp(-\mathrm{i}\boldsymbol{Q} \cdot \boldsymbol{d}) W_d(\boldsymbol{Q}_\perp)$, using the Fourier transform of the window function $W_d(\boldsymbol{Q}_\perp) = \int \mathrm{d}\boldsymbol{r}_\perp \exp(-\mathrm{i}\boldsymbol{Q}_\perp \cdot \boldsymbol{r}_\perp) W_d(-\boldsymbol{r}_\perp)$. To obtain Eq. (B4), $\rho_d(\boldsymbol{r}_\parallel)$ has been simplified to $\delta(\boldsymbol{r}_\parallel)$, which should be replaced by the electron density, or nuclear scattering length, for X-ray and neutron scattering, respectively. As can be seen from the equation, the nuclear Bragg reflections appear at the projected positions of the 6D reciprocal-lattice points, that is, $\boldsymbol{G}_\parallel$. Thus, sets of six integers are required to index the Bragg reflections.

---

* Corresponding address.
** Present address: ISIS facility, Rutherford Appleton Laboratory, Chilton, Didcot, Oxfordshire OX11 0QX, U.K.

[1] D. Shechtman, I. Blech, D. Gratias and J. W. Cahn, Phys. Rev. Lett. **53**, 1951 (1984).
[2] For reviews on quasicrystals, see *Physical Properties of Quasicrystals*, edited by Z. M. Stadnik (Springer-Verlag, Berlin, 1999).
[3] For a review on structure of quasicrystals, see A. Yamamoto, Acta. Crystallogr. Sect. A **52**, 509 (1996).
[4] Y. Achiam, T. C. Lubensky and E. W. Marshall, Phys. Rev. B **33**, 6460 (1986).
[5] H. Tsunetsugu and K. Ueda, Phys. Rev. B **36**, 5493 (1987).

[6] C. Godrèche, J. M. Luck and H. Orland, J. Stat. Phys. **45**, 777 (1986).
[7] H. Aoyama and T. Odagaki, J. Stat. Phys. **48**, 503 (1987).
[8] Y. Okabe and K. Niizeki, in *Quasicrystals*, edited by T. Fujiwara and T. Ogawa (Springer-Verlag, Berlin, 1990), p. 206.
[9] D. Ledue, J. Teillet, J. Carnet and J. Dujardin, J. Non-Cryst. Solids **153&154**, 403 (1993).
[10] R. W. Reid, S. K. Bose and B. Mitrović, J. Phys.: Condens. Matter **10**, 2303 (1998).
[11] R. Lifshitz, Phys. Rev. Lett. **80**, 2717 (1998).
[12] S. Matsuo, H. Nakano, T. Ishimasa and M. Mori, J. Phys. Soc. Jpn. **62**, 4044 (1993).
[13] M. A. Chernikov, A. Bernasconi, C. Beeli, A. Schilling and H. R. Ott, Phys. Rev. B **48**, 3058 (1993).
[14] D. Bahadur, Prog. Cryst. Growth and Charact. **34**, 287 (1997).
[15] Z. Luo, S. Zhang, Y. Tang and D. Zhao, Scripta Metal. Mater. **28**, 1513 (1993).
[16] A. Niikura, A. P. Tsai, A. Inoue and T. Masumoto, Philos. Mag. Lett. **69**, 351 (1994).
[17] A. P. Tsai, A. Niikura, A. Inoue, T. Masumoto, Y. Nishida, K. Tsuda and M. Tanaka, Philos. Mag. Lett. **70**, 169 (1994).
[18] A. Yamamoto, S. Weber, A. Sato, K. Kato, K. Ohshima, A. P. Tsai, A. Niikura, K. Hiraga, A. Inoue and T. Masumoto, Philos. Mag. Lett. **73**, 247 (1996).
[19] T. Ohno and T. Ishimasa, in *Proceedings of the 6th international conference on quasicrystals*, edited by S. Takeuchi and T. Fujiwara (World Scientific, Singapore, 1998) p. 39.
[20] Y. Hattori, A. Niikura, A. P. Tsai, A. Inoue, T. Masumoto, K. Fukamichi, H. Aruga-Katori and T. Goto, J. Phys.: Condens. Matter **7**, 2313 (1995).
[21] B. Charrier and D. Schmitt, J. Magn. Magn. Mater. **171**, 106 (1997).
[22] I. R. Fisher, K. O. Cheon, A. F. Panchula, P. C. Canfield, M. Chernikov, H. R. Ott and K. Dennis, Phys. Rev. B **59**, 308 (1999).
[23] S. Kashimoto, S. Matsuo, H. Nakano, T. Shimizu and T. Ishimasa, Solid State Commun. **109**, 63 (1999).
[24] B. Charrier and D. Schmitt, J. Magn. Magn. Mater. **189**, 165 (1998).
[25] D. R. Noakes, G. M. Kalvius, R. Wäppling, C. E. Stronach, M. F. White Jr., H. Saito and K. Fukamichi, Phys. Lett. A **238**, 197 (1998).
[26] B. Charrier, B. Ouladdiaf and D. Schmitt, Phys. Rev. Lett. **78**, 4637 (1997). The magnetic modulation-vector defined in this paper corresponds to $(\frac{1}{2},0,0,0,0,0)_{\boldsymbol{a}^*}$ using the present definition [56]. The subscript $\boldsymbol{a}^*$ indicates that the vector is defined with the basis vectors of the reciprocal lattice of the 6D hypercubic crystal. See Appendix B for the definitions.
[27] Z. Islam, I. R. Fisher, J. Zarestky, P. C. Canfield, C. Stassis and A. I. Goldman, Phys. Rev. B **57**, R11047 (1998).
[28] T. J. Sato, H. Takakura, A. P. Tsai and K. Shibata, Phys. Rev. Lett. **81**, 2364 (1998)
[29] M. V. Jarić, Phys. Rev. B **34**, 4685 (1986).
[30] V. Elser, Phys. Rev. B **32**, 4892 (1985).
[31] V. Elser, Acta Cryst. A **42**, 36 (1986).
[32] T. J. Sato, H. Takakura, A. P. Tsai, K. Ohoyama, K. Shibata and K. H. Andersen, *Materials Research Society Symposium Proceedings Volume 553: Quasicrystals*, edited by J. M Dubois, P. A. Thiel, A. P. Tsai and K. Urban (Materials Research Society, Pennsylvania, 1999) p. 415.
[33] T. J. Sato, H. Takakura and A. P. Tsai, Jpn. J. Appl. Phys. **37**, L663 (1998).
[34] I. R. Fisher, Z. Islam, A. F. Panchula, K. O. Cheon, M. J. Kramer, P. C. Canfield and A. I. Goldman, Philos. Mag. B **77**, 1601 (1998).
[35] A. Langsdorf and W. Assmus, J. Cryst. Growth **192**, 152 (1998).
[36] K. Ohoyama, T. Kanouchi, K. Nemoto, M. Ohashi, T. Kajitani and Y. Yamaguchi, Jpn. J. Appl. Phys. **37**, 3319 (1998).
[37] O. Schärpf and H. Capellmann, Phys. Stat. Sol. (a) **135**, 359 (1993).
[38] A. P. Murani and A. Heidemann, Phys. Rev. Lett. **41**, 1402 (1978).
[39] A. J. Freeman and J. P. Desclaux, J. Magn. Magn. Mater. **12**, 11 (1979).
[40] S. W. Lovesey, *Theory of neutron scattering from condensed matter* (Clarendon press, Oxford, 1984).
[41] T. J. Sato, H. Kadowaki, H. Yoshizawa, T. Ekino, T. Takabatake, H. Fujii, L. P. Regnault and Y. Isikawa, J. Phys.: Condens. Matter **7**, 8009 (1995).
[42] H. Kadowaki, K. Ubukoshi, K. Hirakawa, J. L. Matrinez and G. Shirane, J. Phys. Soc. Jpn. **56**, 4027 (1987).
[43] We neglect the term, $< \hat{\boldsymbol{T}}^{(\perp)}(\boldsymbol{Q}_{\parallel}) \times \hat{\boldsymbol{T}}^{(\perp)}(-\boldsymbol{Q}_{\parallel}) >$, appearing in the spin-flip scattering, because it is canceled out by the average for the equally populated domains. $\hat{\boldsymbol{T}}^{(\perp)}$ is defined by $\hat{\boldsymbol{T}}^{(\perp)} = \hat{\boldsymbol{T}} - \tilde{\boldsymbol{Q}}(\tilde{\boldsymbol{Q}} \cdot \hat{\boldsymbol{T}})$.
[44] This implicitly assumes the dipole approximation, which is reasonable for the present $\boldsymbol{Q}_{\parallel}$ range.
[45] Below $T_{\rm f}$, the spins may freeze and thus the translational symmetry in the 6D space can probably break. Therefore, we use the spatial average, $< \hat{\boldsymbol{J}}_{0,d} \cdot \hat{\boldsymbol{J}}_{l,d'} >_{\rm A}$, to define the model spin-correlations. Above $T_{\rm f}$ the averaged correlations equal to $< \hat{\boldsymbol{J}}_{n,d} \cdot \hat{\boldsymbol{J}}_{n+l,d} >$, because the system is paramagnetic, and thus, translationally invariant.
[46] In this paper, we have used the Gaussian form of the spin correlations as a trial function, because it is mathematically the simplest and can easily be Fourier-transformed. In the previous paper [28], we used a product of Lorentzian-type correlations. The results for both the functions are qualitatively the same, suggesting that the overall features are independent of the trial functions.
[47] H. Takakura *et al.* to be submitted.
[48] Although a report claims that the Hamiltonian can be transferred to the higher dimensional space; J. P. Lu and J. L.

Birman, Phys. Rev. B **36**, 4471 (1987).
[49] The self-similarity in the Al-TM icosahedral quasicrystals is discussed by C. Janot, J. Phys.: Condens. Matter **9**, 1493 (1997) and references therein.
[50] J. D. Patterson, G. R. Gruzalski and D. J. Sellmyer, Phys. Rev. B **18**, 1377 (1978).
[51] E. M. Chudnovsky, W. M. Saslow and R. A. Serota, Phys. Rev. B **33**, 251 (1986).
[52] S. Matsuo, T. Ishimasa and H. Nakano, *Materials Research Society Symposium Proceedings Volume 553: Quasicrystals*, edited by J. M Dubois, P. A. Thiel, A. P. Tsai and K. Urban (Materials Research Society, Pennsylvania, 1999) p. 427.
[53] A. Jagannathan and H. J. Schulz, Phys. Rev. B **55**, 8045 (1997).
[54] For instance, M. Boudard, M. de Boissieu, C. Janot, G. Heger, C. Beeli, H. -U. Nissen, H. Vincent, R. Ibberson, M. Audier and J. M. Dubois, J. Phys.: Condens. Matter **4**, 10149 (1992).
[55] E. Abe and A. P. Tsai, Phys. Rev. Lett. **83**, 753 (1999). See also the report for the decagonal Zn-Mg-RE systems: E. Abe, T. J. Sato and A. P. Tsai, Phys. Rev. Lett **82**, 5269 (1999).
[56] A. Yamamoto, Phys. Rev. B **45**, 5217 (1992).